PURDUE
UNIVERSITY

DAVIDSON SCHOOL OF CHEMICAL ENGINEERING

Thank you for your interest in my publications!

This article was downloaded from my personal website and for non-commercial purposes only.

If you have any question and/or comment, please contact with me.

Dr. Yang Xiao
Research Associate
Davidson School of Chemical Engineering, Purdue University
West Lafayette, IN 47907-2100, U.S.A
Office: 765-496-3787, Fax: 765-494-0805
E-mail: xiao63@purdue.edu, xiaohaiyi8080@gmail.com
Website:www.xiaohaiyi8080.com

Welcome to access more of my research at www.xiaohaiyi8080.com

I&EC research
Industrial & Engineering Chemistry Research

Article

pubs.acs.org/IECR

Guaiacol Hydrodeoxygenation over Platinum Catalyst: Reaction Pathways and Kinetics

Danni Gao, Yang Xiao, and Arvind Varma*

School of Chemical Engineering, Purdue University, West Lafayette, Indiana 47907, United States

ABSTRACT: Guaiacol represents a large fraction of lignin derived pyrolysis bio-oils. It was shown in our prior work that Pt has higher activity and stability for guaiacol hydrodeoxygenation as compared to other noble metal catalysts. In the present study, further theoretical and experimental investigations were conducted to reveal the reaction pathways and kinetics. For Pt/C catalyst in a fixed-bed reactor, the main liquid phase reaction products were phenol, catechol and cyclopentanone. Because cyclopentanone was typically not observed in the prior literature, a pathway for its formation was proposed and supported by density functional theory (DFT) calculations. By varying the space velocity, kinetic data was acquired in the temperature range 275 to 325 °C. The rate constants and activation energies for each subreaction in the network were obtained based on the power-law model.

1. INTRODUCTION

It has been suggested that, based on the estimated rate of future worldwide energy consumption, the current fossil fuel reserves would last for only a few more decades. Although this forecast is likely to improve due to the availability of newly developing sources, such as shale gas and tar sands, for the longer term there is a need to develop renewable resources for fuels and chemicals production. These candidates would need to meet many performance criteria, some of which are determined in relation to the properties of fossil fuels and others by the existing energy infrastructure tailored toward fossil fuel processing. These factors include competitive pricing, comparable and preferably better carbon efficiency, high expansion capacity and flexible implementation with the existing infrastructure. In light of all these factors, biomass has been shown to be an important renewable energy source.[1]

Fast pyrolysis is an attractive technology to convert biomass to bio-oils, which can subsequently be converted to liquid fuels or chemicals. Oxygen removal from bio-oils, however, remains a major challenge, as high oxygen content lowers its stability and heating value.[2] In this context, hydrodeoxygenation (HDO) is a promising strategy to reduce the oxygen content.[2,3] Processes such as hydrodesulfurization (HDS) and hydrodenitrogenation (HDN) with similar features to HDO, including both hydrogenation and C−X (X = S or N) bond cleavage, have been well studied in the literature. HDO, however, has its own characteristics (kinetics, deactivation and reaction pathways, etc.), which mainly result from C−O bond cleavage, and require more understanding.[3] Extensive research is being carried out in this area, and one of the approaches is to select representative compounds to gain more knowledge about the reaction mechanisms.

Bio-oils are a complex mixture of chemical species, where guaiacol is a good representative of the phenolic group compounds.[4] Its molecular structure contains the two most common oxygenated groups in the lignin-derived bio-oils: hydroxy and methoxy groups. Generally, two types of deoxygenation mechanisms have been proposed: (1) hydrogenation deoxygenation (HYD) in which hydrogenation occurs first and is followed by the removal of oxygen from the saturated hydrocarbon rings, and (2) direct deoxygenation route (DDO), which involves the direct cleavage of the Ar−O bond without ring saturation.[5]

Investigating the HDO activity and understanding the mechanism of different catalyst candidates is a critical part of the research.[6] HDS catalysts (NiMo and CoMo on alumina) exhibit some HDO activity, but lead to significant deactivation and sulfur contamination.[6−9] In our prior work, it was shown that Pt/C catalyst, as compared with Ru, Rh and Pd on carbon catalysts, was able to sufficiently cleave the Ar-OCH_3 bond and produce phenol at high yield (>40%) under atmospheric pressure. The catalyst also demonstrated higher stability with essentially no sign of deactivation for a test period of 5 h, and was found to be a promising candidate for the deoxygenation of guaiacol.[10]

In the present work, to reveal the reaction pathways and kinetics of guaiacol HDO, experimental and theoretical investigations were conducted. The formation of cyclopentanone was observed experimentally and supported by density functional theory calculations. A kinetic study for Pt/C catalyzed guaiacol HDO was carried out, and the rate constants and activation energy values were determined for the individual reaction steps. Limited kinetic studies have been reported previously in this field,[11−13] and the results from this work was compared with the available literature.

2. METHODS

2.1. Experimental. *2.1.1. Materials.* Powder Pt/C, with 5 wt % Pt loading, was purchased from Alfa Aesar. The powder was sieved using a digital sieve shaker (Octagon D200), and particles of size 100 ± 25 μm were used for the experimental study. Guaiacol (>98.0%) and all other chemicals (methanol,

Received: August 10, 2015
Revised: October 9, 2015
Accepted: October 13, 2015
Published: October 13, 2015

DOI: 10.1021/acs.iecr.5b02940
Ind. Eng. Chem. Res. 2015, 54, 10638−10644

phenol, anisole, cresol and catechol) were purchased from Sigma-Aldrich. Ultrahigh purity (99.999%) hydrogen and nitrogen gases were purchased from Indiana Oxygen.

The BET surface area, pore size and metal dispersion by CO adsorption were measured for the fresh catalyst samples using surface area and porosimetry analyzer (ASAP 2000, Micromeritics), and the results are summarized in Table 1.

Table 1. Characterization of Pt/C Catalyst

	Pt/C
BET surface area (m^2/g)	716
pore diameter (Å)	33.7
metal dispersion (%)	36.6

2.1.2. Reaction Apparatus. The experiments were conducted in a continuous flow system similar to that described in our prior work.[10] The catalyst powder was packed in a stainless steel reactor (OD = 12.7 mm, ID = 10.2 mm), with quartz wool plugs placed on both ends. Stainless steel meshes were used on both ends of the quartz wool plugs to hold the catalyst in place and guide the thermocouple into the catalyst bed to measure the bed temperature during reaction. The reactor was heated by a tubular furnace. Gas feed flows were controlled by a set of mass flow controllers (Millipore Tylan 2900) whereas guaiacol feed was controlled using a syringe pump (KDScientific 410). The reaction was conducted in an up-flow configuration, with the guaiacol feed line preheated to 180 °C. A customized double-wall condenser under ice water circulation was used to collect the liquid reaction product, whereas the gaseous products were analyzed on-stream every 10 min. All experiments were conducted under excess hydrogen flow (feed molar ratio of H_2 to guaiacol ~10).

2.1.3. Reaction Product Analysis. The liquid product samples were analyzed by a GC−MS intrument (LECO Pegasus 4D GCxGC-TOF) to identify the composition. The GC−MS was coupled with an autosampler (CTC, GC-xt) and equipped with a DB-WAX column (30 m × 0.32 mm). For routine analysis, the liquid samples were analyzed by a gas chromatograph (Agilent GC6890) equipped with flame ionization detector and a DB-WAX (30 m × 0.32 mm) column. Standard calibration curves were generated for 7 liquid compounds (methanol, phenol, anisole, cyclopentanone, guaiacol, cresol and catechol), with $R^2 > 0.99$ for each curve. ^{13}C NMR analysis of the liquid product was also conducted for some cases, using a Bruker ARX400 instrument.

The gaseous product passing through the condenser was analyzed by a Micro GC (Agilent 3000A Micro GC) equipped with a MolSieve 5A column and a Plot U column. Calibration was performed for hydrogen, nitrogen, methane, carbon monoxide and carbon dioxide.

2.2. Computational. DFT calculations were performed using the periodic plane-wave-based code Vienna Ab-initio Simulation Package (VASP),[14,15] employing the projector augmented wave (PAW)[16,17] method for ionic cores and PW91[18] form of exchange-correlation functional at generalized-gradient approximation level. A cutoff energy of 400 eV was adopted for plane-wave basis whereas a Monkhorst−Pack mesh of 5 × 5 × 1 *k*-points was sampled for the Brillouin zone.[19] In all cases, a first-order Methfessel−Paxton smearing with a width of 0.15 eV was used and the total energies were evaluated by extrapolations to zero broadening.[20]

An ideal Pt(111) surface was represented by a five-layer periodic (3 × 3) unit cell slab model in a supercell geometry with 1.4 nm vacuum spacing between them. During the geometry optimization, the top two layers with the adsorbents were allowed to relax while the other three layers were fixed according to bulk-terminated geometry. The self-consistent iterations were converged with a criterion of 1×10^{-4} eV, and the ionic steps were converged to 0.02 eV/Å. Dipole corrections were included only in the direction perpendicular to slab surface. Spin polarization was applied for gas phase radicals due to the possible presence of unpaired electrons.

The binding energy (BE) is defined as

$$E_{ads} = E_{ad/slab} - E_{ad} - E_{slab}$$

A negative value of BE implies an exothermic process or a favorable interaction, whereas a positive value means an endothermic process or an unfavorable interaction.

To calculate the free energy, zero-point energy corrections were applied to each structure. The entropy correction was performed at 300 °C, and based on the assumption that each adsorbate is a localized oscillator with only vibrational modes.

2.3. Kinetics. Prior to reaction experiments, the catalyst was activated for 4 h under the following conditions: 350 °C, 1 atm, total gas flow 100 mL/min (H_2:N_2 = 1:2). The standard reaction conditions were: 300 °C, 1 atm, 0.5 g catalyst, total gas (H_2:N_2 = 1:1) flow rate 100 mL/min and guaiacol feed rate 0.025 mL/min (liquid, at room temperature). This feed rate corresponds to 9.1 H_2/guaiacol molar ratio, and guaiacol partial pressure 0.052 atm. Both catalyst loading and guaiacol feed rate were varied to acquire data at different residence times. When the gas feed rate was varied, the hydrogen flow rate was adjusted to maintain a constant molar feed ratio, H_2/guaiacol =10.

Before conducting the kinetics study, it is important to ensure the absence of any mass and heat transfer limitations. The absence of mass transfer limitations was verified by using the criteria described by Weisz and Prater,[21] where $\psi < 0.05$ in all cases. To confirm the absence of heat transfer limitations, criteria for fixed-bed reactors proposed by Mears[22] were applied and the results confirmed that there were no intrareactor, interphase or intraparticle heat transfer limitations under the tested conditions.

The calculations for conversion and selectivity were performed based on equations reported in our prior work.[10] The mass balance for each run was above 90%. The accuracy of gas flow measurements was confirmed by evaluating nitrogen balance, with difference between inlet and outlet being less than 3%. Because it is not possible to collect all condensed liquid (liquid drops are visible on the condenser wall), it was reasonable to assume that the total carbon and mass losses were caused by the incomplete liquid product collection. Thus, the product distribution was corrected by assuming that 0.1 g liquid product (equivalent to 2−3 drops) was held in the condenser. After applying this correction, mass balances for all runs were above 96%.

3. RESULTS AND DISCUSSIONS

3.1. Reaction Pathways. *3.1.1. Experimental Confirmation.* In our prior work, the following reaction pathways were proposed and confirmed through experiments for the Pt/C catalyzed guaiacol hydrodeoxygenation reactions (see Figure 1).[10] Reactions 2 and 5 were confirmed using cathechol as a reactant.

DOI: 10.1021/acs.iecr.5b02940
Ind. Eng. Chem. Res. 2015, 54, 10638−10644

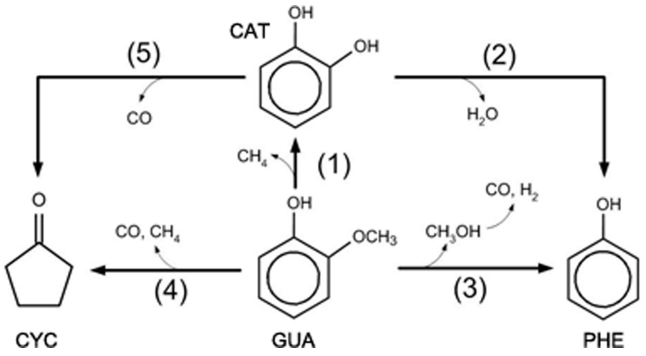

Figure 1. Reaction pathways for Pt/C catalyst.

Remarkably, during guaiacol hydrodeoxygenation studies, cyclopentanone has only been observed a few times by other authors. Its formation depends strongly on the catalyst active metal.[10,23,24] To confirm that cyclopentanone forms during the reaction, an additional analytical method, ^{13}C NMR analysis was performed for the reaction product obtained under standard conditions with Pt/C as catalyst (Figure 2). By comparing the acquired spectrum with NIST database, the three peaks at 224.9, 38.1 and 22.6 ppm confirmed the existence of cyclopentanone. The presence of phenol and catechol, as the other two major reaction products, was also verified in this manner.

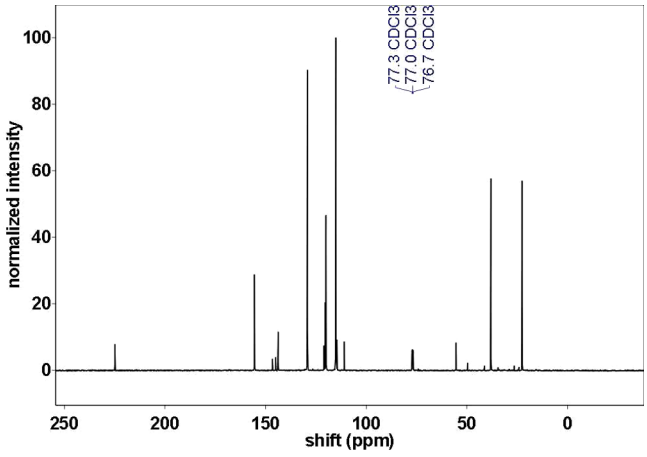

Figure 2. ^{13}C NMR spectra for reaction products (solvent $CDCl_3$).

3.1.2. DFT Calculations. Because cyclopentanone has not been observed often in guaiacol hydrodeoxygenation studies, and it is also unclear how a six-membered ring opens to form a five-membered ring compound, calculations based on density functional theory were performed in an attempt to gain insight into its thermodynamic feasibility. The possible steps for cyclopentanone formation in the reaction system include partial hydrogenation of the aromatic ring; isomerization;[25,26] keto−enol tautomerism;[27] α-diketones decarbonylation[28,29] and ring-closing.[10,30]

Pt(111) surface accounts for most ideal exposed surfaces when the metal particle diameter is ∼3 nm,[31,32] whereas our metal dispersion measurement (see Table 1) corresponds to particle diameter ∼3 nm as well.[33] Although a few articles note that stepped surfaces (e.g., Pt(211)) may play an important role in HDO reaction,[34,35] the main purpose of DFT calculations in the present work was to reveal the formation mechanism of the uncommon five-membered ring product cyclopentanone. To our knowledge, no similar work has been reported previously. For the above reasons, Pt(111) was selected to represent the catalyst surface in this work.[36]

The structure of the Pt bulk was optimized and the lattice constant was found to be 3.99 Å, which is consistent with values reported in the literature and compares well with the experimental value (3.92 Å).[37] On the basis of the proposed steps, the relative free energy levels of each absorbate on Pt at 300 °C were calculated, and the results are presented in Figure 3. Although cyclopentanone can be produced from either guaiacol or catechol (see Figure 1), their reaction mechanisms were similar. Thus, only the results with guaiacol as reactant are presented.

It is noted that after partial hydrogenation, the free energy levels for all following steps decrease, indicating increasing molecule stability. Thus, after the first step the formation of cyclopentanone is thermodynamically feasible. The effect of support is not accounted for because the structure of activated

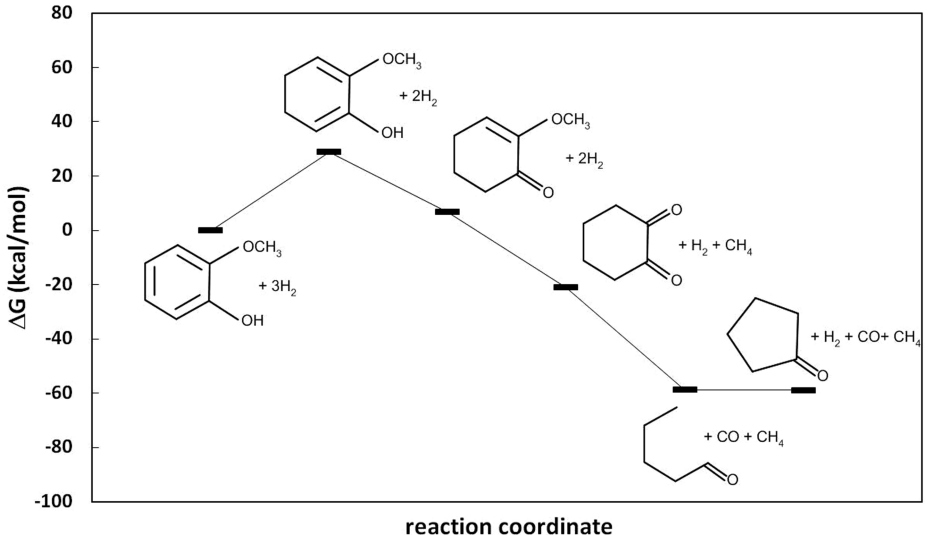

Figure 3. Energy level for reaction coordinate.

DOI: 10.1021/acs.iecr.5b02940
Ind. Eng. Chem. Res. 2015, 54, 10638−10644

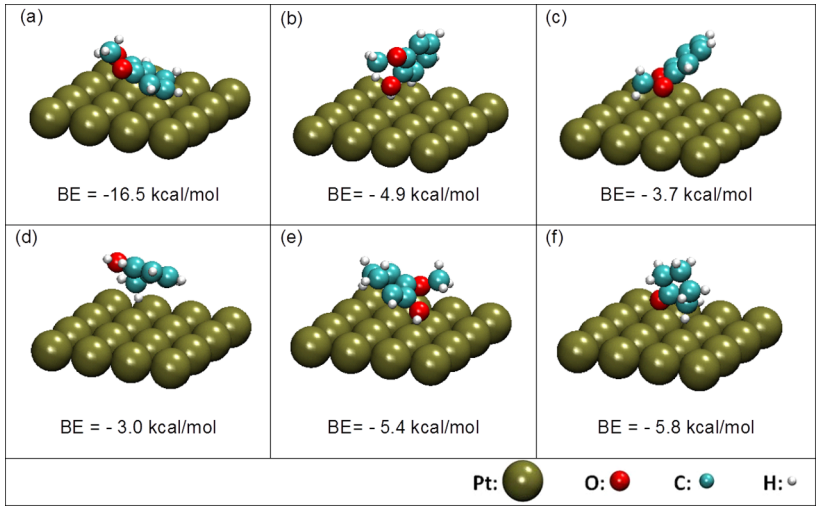

Figure 4. Schematic illustrations of (a–d) guaiacol configurations adsorbed on platinum slabs; (e) the most stable partially hydrogenated intermediate adsorbed on platinum slabs; (f) the most stable cyclopentanone configuration adsorbed on platinum slabs.

carbon is complex and the calculation is computationally expensive, beyond the scope of this work.

To verify the feasibility of the first step, adsorption of guaiacol on Pt cluster was calculated based on DFT to provide information on how the compound interacts with the metal cluster. Several plausible adsorption configurations of guaiacol were constructed and optimized, among which four converged to the desired level (Figure 4a–d). The calculations show that the most stable configuration of adsorbed guaiacol is in a tilted position via the para-carbon (Figure 4a), with the binding energy −16.48 kcal/mol. The other three optimized adsorption positions (Figure 4b–d) are meso-stable with binding energies −4.94, −3.70 and −3.04 kcal/mol, respectively.

For the most stable structure, the Pt–C bond length is 2.15 Å, which indicates chemisorption.[38] The result illustrates that the proposed first step for cyclopentanone formation, i.e., partial hydrogenation, is configurationally possible. It is well-known that hydrogen dissociates rapidly on Pt. Thus, after guaiacol adsorption, the dissociated hydrogen on Pt could diffuse on the metal surface and hydrogenate the C–C bond. The structure for this partially hydrogenated compound was also optimized (Figure 4e). In this case, the oxygen-containing groups, instead of the ring, are adsorbed on metal surface, which could further activate the binding intermediate to react through the steps proposed in Figure 3. The other two main reaction products, catechol and phenol, could be produced from all four adsorbed guaiacol structures on Pt.

Several adsorption configurations of cyclopentanone were also optimized and the most stable one is shown in Figure 4f. The cyclopentanone molecule is adsorbed on the Pt surface through the oxygen, with a binding energy of −5.79 kcal/mol. This implies that the adsorption of cyclopentanone on Pt cluster is weak. Thus, cyclopentanone may desorb rapidly after its formation and has lower probability to react further to other compounds.

3.2. Kinetic Modeling. The guaiacol–hydrogen reaction network (see Figure 1) includes 5 subreactions (eqs 1–5). In this section, kinetic study is performed for the proposed reaction pathways. To acquire the experimental data, space velocity was varied by changing both guaiacol feed rate and catalyst weight at three temperatures (275, 300 and 325 °C) under integral operating conditions.

$$\mathrm{GUA} + \mathrm{H_2} \xrightarrow{k_1} \mathrm{CAT} + \mathrm{CH_4} \quad (1)$$

$$\mathrm{CAT} + \mathrm{H_2} \xrightarrow{k_2} \mathrm{PHE} + \mathrm{H_2O} \quad (2)$$

$$\mathrm{GUA} + 2\mathrm{H_2} \xrightarrow{k_3} \mathrm{PHE} + \mathrm{MeOH} \quad (3)$$

$$\mathrm{GUA} + 3\mathrm{H_2} \xrightarrow{k_4} \mathrm{CYC} + \mathrm{CO} + \mathrm{CH_4} \quad (4)$$

$$\mathrm{CAT} + 2\mathrm{H_2} \xrightarrow{k_5} \mathrm{CYC} + \mathrm{CO} \quad (5)$$

Three common kinetic models (i.e., power-law, Langmuir–Hinshelwood and Rideal–Eley) were evaluated. For the two adsorption based models, a large number of parameters exist which may significantly decrease the reliability of the data fitting. Also, after applying several adsorption/dissociative mechanisms in attempts to describe the experimental values, the results were unsatisfactory. When the power-law kinetics model was applied, however, good fitting results and reasonable kinetic parameters were obtained. Therefore, the power-law kinetic model was selected to describe the reaction system.

First, guaiacol conversion was evaluated to obtain the reaction order for eqs 1, 3 and 4. The design equation for a plug-flow packed-bed reactor was integrated based on the assumption that the reaction order was zero, one, two or three. The results showed that good fitting was achieved when the reaction order was 2 (Figure 5). Thus, a second-order model appears to be appropriate to describe guaiacol conversion. Runnebaum et al. have proposed a first-order model for guaiacol conversion, when Pt/Al_2O_3 was tested under differential conditions.[11] For the present work, however, the fitting results based on second-order kinetics were best.

Therefore, reactions 1, 3 and 4 are assumed to be second order with respect to guaiacol. Different reaction orders were also investigated for reactions 2 and 5, and first-order with respect to catechol provided the best fitting results.

On the basis of the design equation for the packed-bed reactor and the reaction network, the formation/consumption rates for each of the major components are listed in eqs 6–9. Because excess hydrogen is used, its partial pressure can be considered constant during the entire reaction and lumped into the rate constants. For given initial conditions, these differential

DOI: 10.1021/acs.iecr.5b02940
Ind. Eng. Chem. Res. 2015, 54, 10638–10644

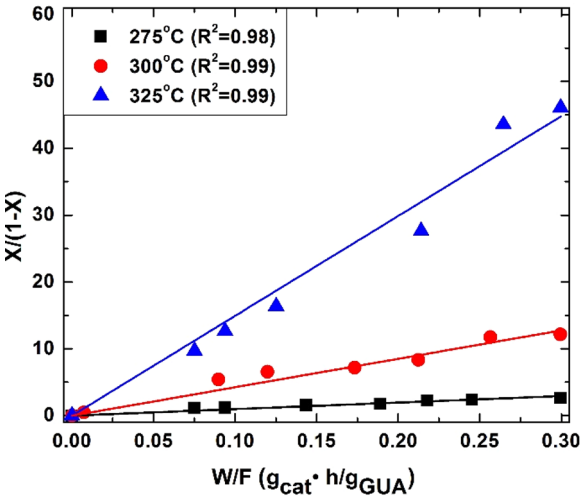

Figure 5. Fitting results of guaiacol conversion (x) based on second-order kinetics.

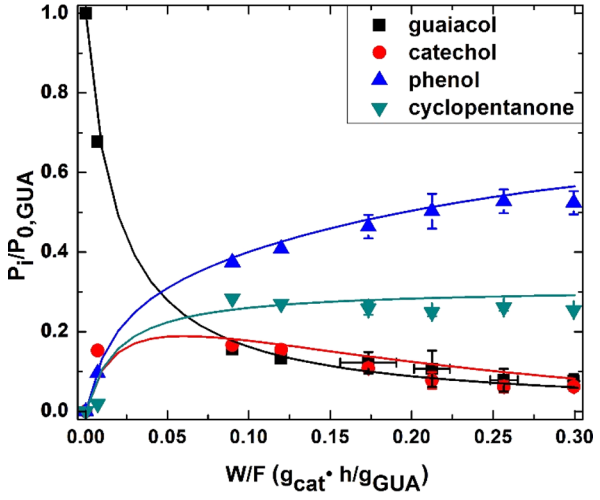

Figure 6. Fit of kinetic data at 300 °C.

equations were solved using the MATLAB ode45s subroutine. The calculated concentration profiles as functions of the residence time were then compared with the experiment data. By minimizing the difference between the calculated and experimental results, the optimum kinetic parameters were determined using the nonlinear fitting subroutine fmincon. To increase the accuracy of mathematical fitting, during the process, partial pressures for all compounds were normalized based on the initial guaiacol partial pressure.

$$\frac{dF_{GUA}}{dW} = -r_1 - r_3 - r_4 \quad (6)$$

$$\frac{dF_{CAT}}{dW} = r_1 - r_2 - r_5 \quad (7)$$

$$\frac{dF_{PHE}}{dW} = r_2 + r_3 \quad (8)$$

$$\frac{dF_{CYC}}{dW} = r_4 + r_5 \quad (9)$$

The method was applied to the three investigated temperatures (275, 300 and 325 °C) separately to acquire the reaction rate constants. Figure 6, which is typical, shows the normalized partial pressures at 300 °C with respect to the inverse space velocity. Good agreement was obtained between the experimental data (represented by points) and the calculated results (represented by curves) for all cases.

Figure 7 summarizes the goodness of fit in a parity plot for each component at all three temperatures. The values for all components are close to the diagonal line and relatively evenly distributed on both sides, indicating good fit. The obtained rate constants are listed in Table 2.

On the basis of the obtained rate constants at different temperatures, the activation energies for the various reactions were calculated. Using Arrhenius law and linear regression (Figure 8), activation energies for the five subreactions were obtained, and the results are listed in Table 3 along with the corresponding R^2 values.

Direct consumption of guaiacol occurs in reactions 1, 3 and 4 and forms catechol, phenol and cyclopentanone, respectively. The rate constants obtained for the three reactions are in the same order of magnitude. The results show that although k_3 is

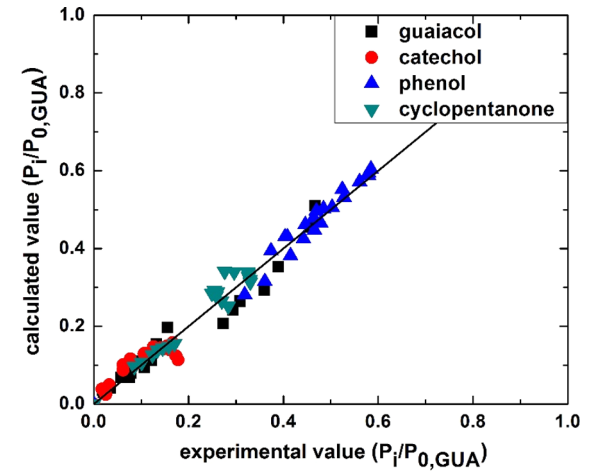

Figure 7. Parity plot for major compounds at 275, 300 and 325 °C.

Table 2. Reaction Rate Constants

temperature	275 °C	300 °C	325 °C
$k_1 \times 10^{-4}$ ($g_{GUA}/(g_{cat}\cdot h\cdot atm^2)$)	0.14	0.70	1.37
$k_2 \times 10^{-2}$ ($g_{CAT}/(g_{cat}\cdot h)$)	0.31	1.05	1.94
$k_3 \times 10^{-4}$ ($g_{GUA}/(g_{cat}\cdot h\cdot atm^2)$)	0.31	0.86	1.71
$k_4 \times 10^{-4}$ ($g_{GUA}/(g_{cat}\cdot h\cdot atm^2)$)	0.11	0.70	1.67
$k_5 \times 10^{6}$ ($g_{CAT}/(g_{cat}\cdot h)$)	0.59	1.67	5.85

almost 2 times as large as k_1 and k_4 at 275 °C, it becomes similar to k_1 and k_4 at 325 °C because of its lower activation energy. Regarding catechol consumption, it is noted that k_2 is much larger than k_5, indicating that the majority of the reacted catechol forms phenol.

The apparent activation energy of guaiacol reaction was also calculated for comparison with literature values. On the basis of the values of k_1, k_3 and k_4 obtained at the three temperatures, the value was determined to be 116.8 kJ/mol. It is higher than the values reported for Co−Mo, Ni−Mo and Ni−Cu catalysts, which are 71.2, 58.7 and 89.1 kJ/mol, respectively,[12,39] and those reported for a series of metal phosphide catalysts, which are in the range of 40−65 kJ/mol.[13] The difference is likely due to the catalyst nature (noble metal versus others), which leads to different reaction pathways and deactivation profiles, since it has been reported that the formation of condensed-ring

DOI: 10.1021/acs.iecr.5b02940
Ind. Eng. Chem. Res. 2015, 54, 10638−10644

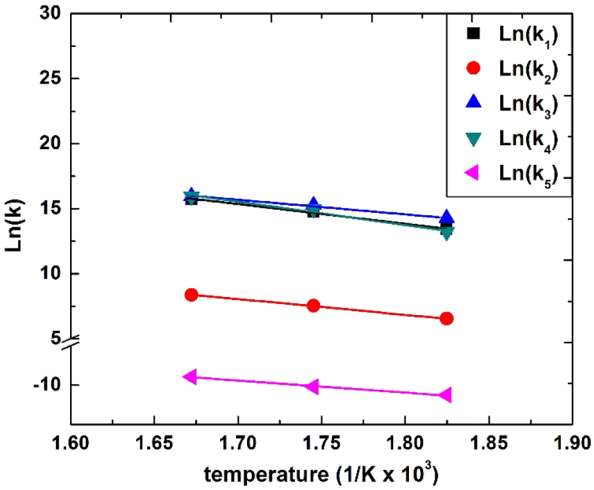

Figure 8. Arrhenius plots for the rate constants.

Table 3. Activation Energy Values

	E_1	E_2	E_3	E_4	E_5
activation energy (kJ/mol)	125.5	99.8	92.7	149.0	124.6
R^2 value	0.98	0.98	0.99	0.98	0.99

compounds has lower activation energy as compared to hydrogenation and oxygenation reactions.[12] Owing to the lack of literature data for Pt catalyst, the activation energy value reported in this work cannot be compared directly.

On the basis of the data analysis, the consumption of guaiacol appears to be second-order. A possible explanation is that under the operating conditions, adsorption of guaiacol is the rate controlling step. Liu and Shen have derived the adsorption rate equation based on Langmuir kinetics, and found that depending on the relative values of initial concentration, maximum adsorption capacity, dosage of adsorbent and equilibrium constant, the adsorption rate may appear to be second order with respect to the adsorbate.[40] This could explain the apparent second-order reaction for guaiacol conversion observed in this study.

4. CONCLUSIONS

For the guaiacol HDO reaction, Pt supported on activated carbon was investigated under atmospheric pressure in a fixed-bed reactor. A possible reaction mechanism starting from the adsorption of guaiacol on catalyst support was proposed. Further, the reaction pathways were investigated through experiments. Plausible reaction steps for cyclopentanone generation from guaiacol were proposed via DFT calculations. Finally, reaction kinetics study was conducted under integral conditions at three temperatures (275, 300 and 325 °C). The power-law model was found to describe the kinetics well, and the rate constants and activation energies were obtained for all subreactions in the network. This experimental and theoretical study provides insight into Pt-catalyzed guaiacol hydrodeoxygenation, and provides a basis for investigations of other phenolic compounds present in pyrolysis bio-oils.

AUTHOR INFORMATION

Corresponding Author

*A. Varma. Telephone: +1-(765) 494-4075. Fax: +1-(765) 494-0805. E-mail: avarma@purdue.edu.

Notes

The authors declare no competing financial interest.

ACKNOWLEDGMENTS

This work was supported by the R. Games Slayter Discretionary Fund. Danni Gao is grateful to Phillips 66 for award of a fellowship. The authors also thank Dr. Kendall Thomson for valuable discussions regarding the computational work, Dr. Jeffery Greeley for providing the computational resources, Yanran Cui for measuring the metal dispersion, and Yucheng Wang for help with the kinetics experiments.

NOMENCLATURE

CAT = catechol
CYC = cyclopentanone
E = activation energy, kJ/mol
F = flow rate, cc/min
GUA = guaiacol
k_i = reaction rate constant
P_i = partial pressure for species i, atm
PHE = phenol
W = catalyst weight, g
x = guaiacol conversion

REFERENCES

(1) Nigam, P. S.; Singh, A. Production of liquid biofuels from renewable resources. *Prog. Energy Combust. Sci.* **2011**, *37*, 52−68.
(2) Elliott, D. C. Historical developments in hydroprocessing bio-oils. *Energy Fuels* **2007**, *21*, 1792−1815.
(3) Furimsky, E. Catalytic hydrodeoxygenation. *Appl. Catal., A* **2000**, *199*, 147−190.
(4) Elliott, D. C.; Hart, T. R. Catalytic Hydroprocessing of Chemical Models for Bio-oil. *Energy Fuels* **2009**, *23*, 631−637.
(5) Nie, L.; Resasco, D. E. Kinetics and mechanism of m-cresol hydrodeoxygenation on a Pt/SiO_2 catalyst. *J. Catal.* **2014**, *317*, 22−29.
(6) Mortensen, P. M.; Grunwaldt, J. D.; Jensen, P. A.; Knudsen, K. G.; Jensen, A. D. A review of catalytic upgrading of bio-oil to engine fuels. *Appl. Catal., A* **2011**, *407*, 1−19.
(7) Wildschut, J.; Mahfud, F. H.; Venderbosch, R. H.; Heeres, H. J. Hydrotreatment of Fast Pyrolysis Oil Using Heterogeneous Noble-Metal Catalysts. *Ind. Eng. Chem. Res.* **2009**, *48*, 10324−10334.
(8) Deepa, A. K.; Dhepe, P. L. Function of Metals and Supports on the Hydrodeoxygenation of Phenolic Compounds. *ChemPlusChem* **2014**, *79*, 1573−1583.
(9) Hellinger, M.; Carvalho, H. W. P.; Baier, S.; Wang, D.; Kleist, W.; Grunwaldt, J. D. Catalytic hydrodeoxygenation of guaiacol over platinum supported on metal oxides and zeolites. *Appl. Catal., A* **2015**, *490*, 181−192.
(10) Gao, D.; Schweitzer, C.; Hwang, H. T.; Varma, A. Conversion of guaiacol on noble metal catalysts: reaction performance and deactivation studies. *Ind. Eng. Chem. Res.* **2014**, *53*, 18658−18667.
(11) Runnebaum, R. C.; Nimmanwudipong, T.; Block, D. E.; Gates, B. C. Catalytic conversion of compounds representative of lignin-derived bio-oils: a reaction network for guaiacol, anisole, 4-methylanisole, and cyclohexanone conversion catalysed by Pt/γ-Al_2O_3. *Catal. Sci. Technol.* **2012**, *2*, 113−118.
(12) Bykova, M. V.; Zavarukhin, S. G.; Trusov, L. I.; Yakovlev, V. A. Guaiacol hydrodeoxygenation kinetics with catalyst deactivation taken into consideration. *Kinet. Catal.* **2013**, *54*, 40−48.
(13) Zhao, H. Y.; Li, D.; Bui, P.; Oyama, S. T. Hydrodeoxygenation of guaiacol as model compound for pyrolysis oil on transition metal phosphide hydroprocessing catalysts. *Appl. Catal., A* **2011**, *391*, 305−310.
(14) Kresse, G.; Hafner, J. Ab-Initio Molecular-Dynamics Simulation of the Liquid-Metal Amorphous-Semiconductor Transition in

DOI: 10.1021/acs.iecr.5b02940
Ind. Eng. Chem. Res. 2015, 54, 10638−10644

Germanium. *Phys. Rev. B: Condens. Matter Mater. Phys.* **1994**, *49*, 14251−14269.
(15) Kresse, G.; Furthmuller, J. Efficiency of ab-initio total energy calculations for metals and semiconductors using a plane-wave basis set. *Comput. Mater. Sci.* **1996**, *6*, 15−50.
(16) Kresse, G.; Joubert, D. From ultrasoft pseudopotentials to the projector augmented-wave method. *Phys. Rev. B: Condens. Matter Mater. Phys.* **1999**, *59*, 1758−1775.
(17) Blochl, P. E. Projector Augmented-Wave Method. *Phys. Rev. B: Condens. Matter Mater. Phys.* **1994**, *50*, 17953−17979.
(18) Perdew, J. P.; Chevary, J. A.; Vosko, S. H.; Jackson, K. A.; Pederson, M. R.; Singh, D. J.; Fiolhais, C. Atoms, Molecules, Solids, and Surfaces - Applications of the Generalized Gradient Approximation for Exchange and Correlation. *Phys. Rev. B: Condens. Matter Mater. Phys.* **1992**, *46*, 6671−6687.
(19) Monkhorst, H. J.; Pack, J. D. Special Points for Brillouin-Zone Integrations. *Phys. Rev. B* **1976**, *13*, 5188−5192.
(20) Methfessel, M.; Paxton, A. T. High-Precision Sampling for Brillouin-Zone Integration in Metals. *Phys. Rev. B: Condens. Matter Mater. Phys.* **1989**, *40*, 3616−3621.
(21) Weisz, P. B.; Prater, C. D. Interpretation of Measurements in Experimental Catalysis. *Adv. Catal.* **1954**, *6*, 143−196.
(22) Mears, D. E. Diagnostic Criteria for Heat Transport Limitations in Fixed Bed Reactors. *J. Catal.* **1971**, *20*, 127−131.
(23) Nimmanwudipong, T.; Aydin, C.; Lu, J.; Runnebaum, R. C.; Brodwater, K. C.; Browning, N. D.; Block, D. E.; Gates, B. C. Selective Hydrodeoxygenation of Guaiacol Catalyzed by Platinum Supported on Magnesium Oxide. *Catal. Lett.* **2012**, *142*, 1190−1196.
(24) Bykova, M. V.; Ermakov, D. Y.; Kaichev, V. V.; Bulavchenko, O. A.; Saraev, A. A.; Lebedev, M. Y.; Yakovlev, V. A. Ni-based sol-gel catalysts as promising systems for crude bio-oil upgrading: Guaiacol hydrodeoxygenation study. *Appl. Catal., B* **2012**, *113*, 296−307.
(25) Smith, H. A.; Stump, B. L. Study of Catalytic Hydrogenation of Hydroxybenzenes over Platinum and Rhodium Catalysts. *J. Am. Chem. Soc.* **1961**, *83*, 2739−2743.
(26) Zhao, C.; He, J. Y.; Lemonidou, A. A.; Li, X. B.; Lercher, J. A. Aqueous-phase hydrodeoxygenation of bio-derived phenols to cycloalkanes. *J. Catal.* **2011**, *280*, 8−16.
(27) Effenber, F. Chemistry of Enol Ethers. *Angew. Chem., Int. Ed. Engl.* **1969**, *8*, 295−312.
(28) Osamura, Y.; Schaefer, H. F.; Dupuis, M.; Lester, W. A. A unimolecular reaction ABC→A+B+C involving three product molecules and a single transition state. Photodissociation of glyoxal: HCOHCO→H_2+CO+CO. *J. Chem. Phys.* **1981**, *75*, 5828−5836.
(29) Jayamani, M.; Pillai, C. N. Reactions of Benzoin and Benzil over Alumina - Decarbonylation of Alpha-Diketones. *J. Catal.* **1985**, *92*, 422−425.
(30) Sudarsanam, P.; Katta, L.; Thrimurthulu, G.; Reddy, B. M. Vapor phase synthesis of cyclopentanone over nanostructured ceria-zirconia solid solution catalysts. *J. Ind. Eng. Chem.* **2013**, *19*, 1517−1524.
(31) Kinoshita, K. Particle-Size Effects for Oxygen Reduction on Highly Dispersed Platinum in Acid Electrolytes. *J. Electrochem. Soc.* **1990**, *137*, 845−848.
(32) Shekhar, M.; Wang, J.; Lee, W. S.; Williams, W. D.; Kim, S. M.; Stach, E. A.; Miller, J. T.; Delgass, W. N.; Ribeiro, F. H. Size and Support Effects for the Water-Gas Shift Catalysis over Gold Nanoparticles Supported on Model Al2O3 and TiO2. *J. Am. Chem. Soc.* **2012**, *134*, 4700−4708.
(33) Ertl, G.; Knözinger, H.; Schüth, F.; Weitkamp, J. *Handbook of heterogenous catalysis*; John Wiley & Sons: New York, 2008.
(34) Lu, J.; Behtash, S.; Mamun, O.; Heyden, A. Theoretical Investigation of the Reaction Mechanism of the Guaiacol Hydrogenation over a Pt(111) Catalyst. *ACS Catal.* **2015**, *5*, 2423−2435.
(35) Lausche, A. C.; Falsig, H.; Jensen, A. D.; Studt, F. Trends in the Hydrodeoxygenation Activity and Selectivity of Transition Metal Surfaces. *Catal. Lett.* **2014**, *144*, 1968−1972.
(36) Honkela, M. L.; Bjork, J.; Persson, M. Computational study of the adsorption and dissociation of phenol on Pt and Rh surfaces. *Phys. Chem. Chem. Phys.* **2012**, *14*, 5849−5854.
(37) Liu, B.; Greeley, J. Decomposition Pathways of Glycerol via C-H, O-H, and C-C Bond Scission on Pt(111): A Density Functional Theory Study. *J. Phys. Chem. C* **2011**, *115*, 19702−19709.
(38) Demuth, J. E.; Jepsen, D. W.; Marcus, P. M. Chemisorption Bonding of C(2 by 2) Chalcogen Overlayers on Ni(001). *Phys. Rev. Lett.* **1973**, *31*, 540−542.
(39) Laurent, E.; Delmon, B. Study of the Hydrodeoxygenation of Carbonyl, Carboxylic and Guaiacyl Groups over Sulfided CoMo/γ-Al2O3 and NiMo/γ-Al_2O_3 Catalyst 0.2. Influence of Water, Ammonia and Hydrogen-Sulfide. *Appl. Catal., A* **1994**, *109*, 97−115.
(40) Liu, Y.; Shen, L. From Langmuir Kinetics to First- and Second-Order Rate Equations for Adsorption. *Langmuir* **2008**, *24*, 11625−11630.

DOI: 10.1021/acs.iecr.5b02940
Ind. Eng. Chem. Res. 2015, 54, 10638−10644